# Polarization Raman spectra of graphene nanoribbons

Wangwei Xu(许望伟)[1,†], Shijie Sun(孙诗杰)[1,†], Muzi Yang(杨慕紫)[2], Zhenliang Hao(郝振亮)[1], Lei Gao(高蕾)[3], Jianchen Lu(卢建臣)[1], Jiasen Zhu(朱嘉森)[2], Jian Chen(陈建)[2,‡], and Jinming Cai(蔡金明)[1,§]

[1] *Faculty of Materials Science and Engineering, Kunming University of Science and Technology, Kunming* 650000, *China*
[2] *School of Materials Science and Engineering, Instrumental Analysis and Research Center, Sun Yat-sen University, Guangzhou* 510275, *China*
[3] *Faculty of Science, Kunming University of Science and Technology, Kunming* 650000, *China*

(Received 29 April 2022; revised manuscript received 23 June 2022; accepted manuscript online 13 July 2022)

The on-surface synthesis method allows the fabrication of atomically precise narrow graphene nanoribbons (GNRs), which bears great potential in electronic applications. Here, we synthesize armchair graphene nanoribbons (AGNRs) and chevron-type graphene nanoribbons (CGNRs) array on a vicinal Au(11 11 12) surface using 10,10′-dibromo-9,9′-bianthracene (DBBA) and 6,12-dibromochrysene (DBCh) as precursors, respectively. This process creates spatially well-aligned GNRs, as characterized by scanning tunneling microscopy. AGNRs show strong Raman linear polarizability for application in optical modulation devices. Different from the distinct polarization of AGNRs, only weak polarization exists in CGNRs polarized Raman spectrum, which suggests that the presence of the zigzag boundary in the nanoribbon attenuates the polarization rate as an important factor affecting the polarization. We analyze the Raman activation mode of CGNRs using the peak polarization to expand the application of the polarization Raman spectroscopy in nanoarray analysis.

**Keywords:** graphene nanoribbons, polarization Raman spectroscopy, scanning tunneling microscopy

**PACS:** 68.37.Ef, 74.25.nd, 78.67.Wj, 81.05.ue **DOI:** 10.1088/1674-1056/ac80b3

## 1. Introduction

Compared with semi-metallic graphene, subnanoscale graphene nanoribbons can open a bandgap of more than 1 eV due to quantum confinement effects, making it possible for GNRs to be applied in semiconductor transistor devices.[1,2] The electronic structures of the GNRs are determined by their atomic structures, which means engineering the width and edge structures can tune the electronic properties of GNRs.[3–6] The bottom-up fabrication provides a method for the preparation of atomically accurate GNRs, making it possible to control the array alignment of GNRs precisely.[7–11] Therefore, we need to synthesize highly aligned GNRs rather than randomly oriented GNRs to fabricate nanodevices such as optical demodulators and field-effect transistors.

Previous work demonstrated that depositing Au gratings on the surface of monolayer graphene to form strip array devices exhibits excellent optical modulation performance.[12] Preparation of GNRs arrays by chemical reaction on periodic step substrates is more accurate and faster than fabrication of gratings on single-layer graphene. The vicinal surfaces of Au (788) and Au (11 11 12) are lined with Au (111) steps that provide a template for growing GNRs arrays.[13–15] In nanodevices, the substrate of GNRs is not the Au substrate but an insulating substrate, such as $SiO_2$. In this case, an effective method is required to characterize the alignment of the arrays before and after the transfer of GNRs. It has been reported that polarized Raman spectroscopy is an effective detection method for armchair GNRs.[14,16] Since the Raman G mode intensity at the armchair edge is proportional to $\cos^2\theta$, the polarization Raman spectra of the AGNRs arrays show evident polarization.[17] The polarization degree before and after the transfer can show the preservation of the arrays during the transfer process. Nevertheless, the polarization Raman studies of graphene nanoribbons with different boundary structures are still not clearly revealed.

On the other hand, Raman spectroscopy, as a widely used characterization, is fast and sensitive to carbon skeleton structure, which makes it particularly well suit to investigating the morphology of carbon materials at the nanoscale.[18,19] However, almost all current polarized Raman spectra of GNRs arrays are characterized by the arrangement of their arrays.[14,15] We believe that the application of GNRs polarization Raman should not be limited to this. Considering that many kinds of Raman active modes of GNRs have polarization effects theoretically,[20,21] we expect that the polarized Raman spectra of GNRs arrays can help us analyze the Raman active mode of complex GNRs, which is a promising application.

To investigate whether the polarization Raman spectrum characterizes GNRs, array arrangement applies to all GNRs and expands other potential applications of polarization Ra-

[†]These authors contributed equally to this work.
[‡]Corresponding author. E-mail: puscj@mail.sysu.edu.cn
[§]Corresponding author. E-mail: j.cai@kust.edu.cn

© 2023 Chinese Physical Society and IOP Publishing Ltd 

man spectrum. The overall experimental exploration scheme is shown in Fig. 1(a). We synthesized AGNRs and CGNRs arrays on Au (11 11 12) surfaces. We measured the polarized Raman spectra of both two kinds of GNRs arrays. The polarization Raman spectrum of AGNRs shows evident polarization in all kinds of Raman peaks, while the polarization Raman spectrum of CGNRs only has weak polarization. We also discovered that the polarization mode of the Raman peak in the polarization Raman spectrum of CGNRs is related to the edge structure of CGNRs.

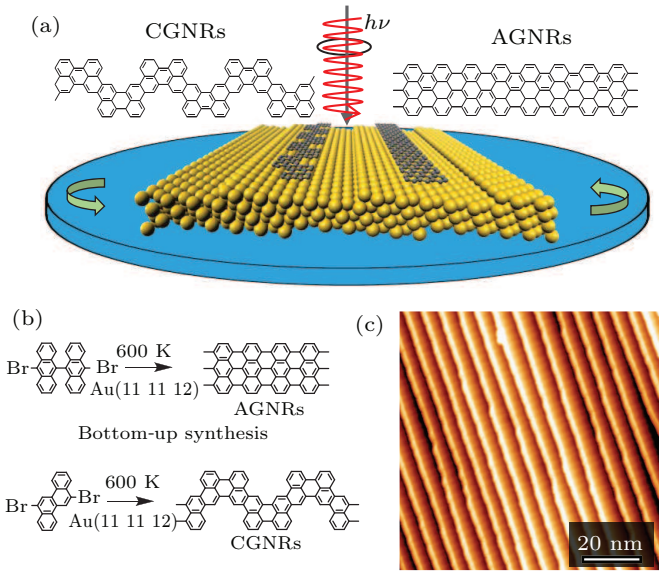



**Fig. 1.** Schematic diagram and substrate. (a) Schematic of different GNR polarized Raman spectrum measurements. (b) Bottom-up synthesis method of AGNRs and CGNRs. (c) STM image of the Au(11 11 12) surface with periodic terrace, $I_t = 25$ pA, $U_s = 1$ V. The surface was cleaned by $Ar^+$ sputtering and annealing before measurement.

## 2. Results and discussion

We prepared graphene nanoribbon arrays on Au (11 11 12) surfaces using DBBA and DBCh organic precursors, respectively. Figure 1(b) illustrates the reaction path of the fabrication of two kinds of GNRs. Spatially aligned GNRs were fabricated on a clean vicinal Au (11 11 12) surface (Fig. 1(c)) under ultra-high vacuum conditions, which promotes GNRs to grow with the [11$\bar{2}$] crystal orientation and arranged in parallel on unidirectional steps. Considering that GNRs arrays are fully layered, we need reaction conditions that allow the free diffusion of the precursor. Instead of holding the substrate at room temperature, we deposited the precursor on Au (11 11 12) held at 470 K, which allows the precursor to debromination and diffuse to form polymers once they reach the substrate.[22] Further annealing to 600 K induces cyclo-dehydrogenation, resulting in AGNRs and chevron CGNRs. Previous literature reported that the length and integrity of GNRs arrays grown on Au (7 8 8) still need to be improved.[13,16,23] We chose Au (11 11 12) as the substrate instead of Au (7 8 8) because Au (11 11 12) has wider steps than Au (7 8 8), which is more conducive to the diffusion of molecules in the reaction. The large-scale high-quality GNRs arrays were fabricated by typically bottom-up synthesis method.

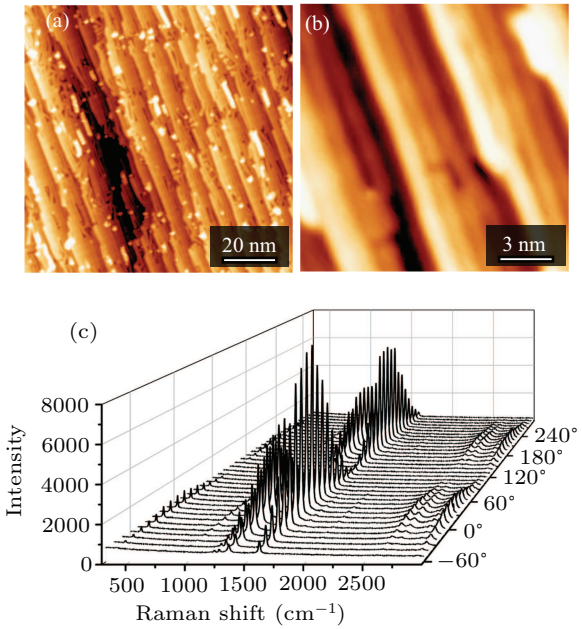



**Fig. 2.** Morphology and polarization Raman analysis of AGNR. (a) The topographic STM image after the growth of the AGNRs, $I_t = 25$ pA, $U_s = 1$ V. (b) A zoom-in image clearly shows the second layer of AGNRs with serrated edges, $I_t = 25$ pA, $U_s = 1$ V. (c) Polarized Raman spectrum of AGNRs.

The AGNRs grow along with the surface steps (Fig. 2(a)) and the average length of the nanoribbons is about 30 nm. The small-scale and high-resolution Fig. 2(b) shows a clear parallel arrangement of single AGNRs in an array distribution. There are multiple nanoribbons on each step, still neatly aligned along the edges. We can see some structures shorter and brighter than AGNRs, which are the second layer of polymers formed by excess molecules. The few second-layer GNRs are challenging to eliminate. Decreasing the deposition rate of precursor molecules will form short GNRs due to the insufficient number of monomers coupled into polymers and AGNRs would grow with the step platform of Au (111).[1] We control the appropriate deposition rate to prepare neat GNR array samples for Raman testing. The polarized Raman spectra of AGNRs at 10° intervals (Fig. 2(c)) show the significantly polarized of each Raman peak. The Raman peaks are strongest only when the linear light is parallel to the GNRs array and weak peaks can be observed. Light irradiation will damage the structure of the AGNRs array, leading the Raman peak intensity to decrease exponentially with irradiation time. Thus, we modified the G peak intensity according to that the peak intensity at 0° and 360° should be the same. Theoretically, the attenuation of the Raman peak caused by light irradiation has no selectivity, so the compensation formula should be applied to all peaks. We have modified the intensity of four peaks and

found that they could use the same equation. Moreover, the intensity polarization diagram of these four peaks is very similar, as shown in Figs. 3(b)–3(d). The four Raman peaks have completely different vibration modes but the same polarization pattern. AGNRs are regarded as a one-dimensional material and the specific vibration mode has no evident influence on polarization indicating that Raman polarization is caused by the size effect.

When the light and the AGNRs array are parallel or vertical, the peak intensity ratio of $G_{\parallel}/G_{\perp}$ reaches 14, while other peaks have a similar enhancement in the case of parallel. Thus, we obtained an enhanced Raman spectrum when the light was parallel to the AGNRs array, as shown in Fig. 3(a). In this enhanced Raman spectrum, we can clearly distinguish various Raman modes. The most active peak is around 1600 $cm^{-1}$, known as the G peak. In graphene, the G band is associated with the doubly degenerate (iTO and LO) phonon mode ($E_{2g}$ symmetry) at the Brillouin zone center.[24] But in AGNRs, only LO mode is Raman active.[25] Between 1200 $cm^{-1}$ and 1400 $cm^{-1}$, there are three distinct Raman peaks, all of which are associated with the edges of the nanoribbons.[26] The low-frequency part of the spectrum is contributed by the radial breathing-like mode (RBLM) with a frequency that scales with ribbon width.[26–28] The peak at 397 $cm^{-1}$ is RBLM, while the peak at 955 $cm^{-1}$ is RBLM-3. We can also observe several double resonance Raman peaks, which are Raman modes of GNRs that have been rarely studied. We have identified several two-phonon bands in Table 1. The wavenumber of second-order Raman peaks of the nanoribbons is equal to the sum of the wavenumbers of the two first-order peaks, which is the same as that of graphene.[28–30] All observed second-order Raman peaks are caused by the resonance of the vibrations of the C atom, which indicates the selection rule of the double resonance Raman mode in GNRs. This enhanced Raman spectroscopy provides an experimental result for the further study of GNRs double resonance Raman.

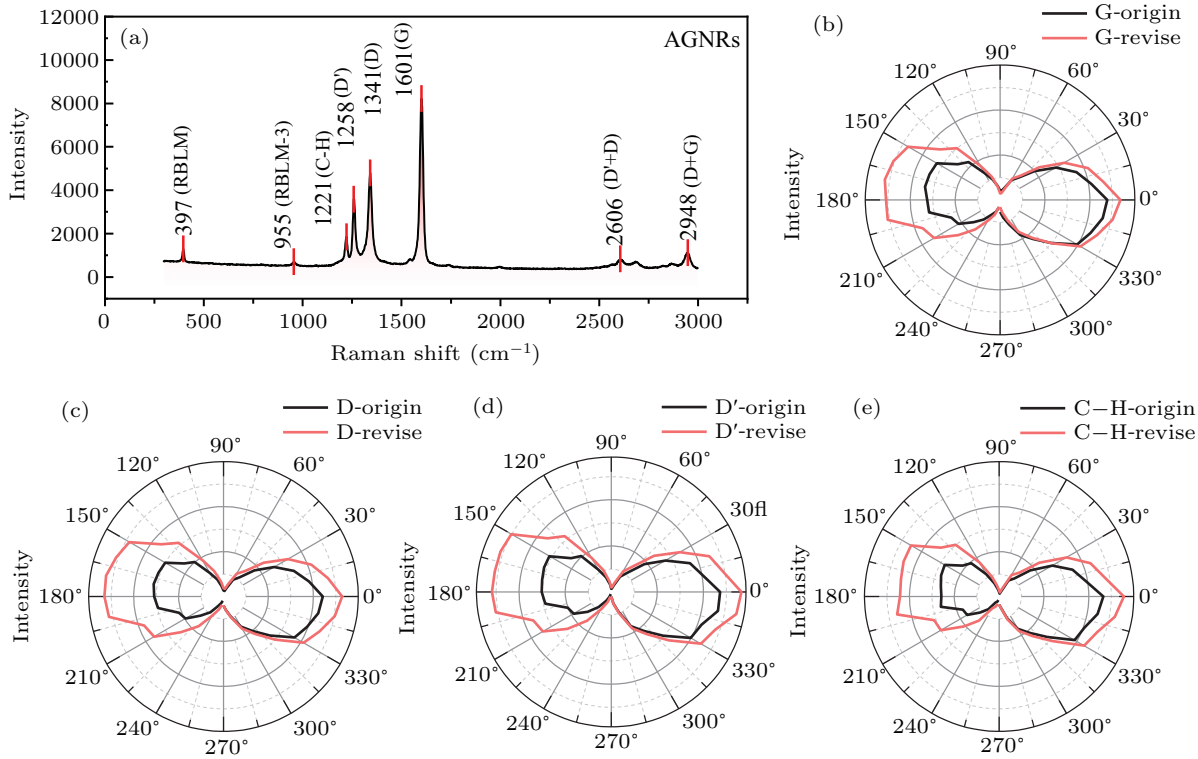



**Fig. 3.** Polarization analysis of different peaks. (a) Enhanced Raman spectra of AGNRs, the polarization of light parallel to the nanoribbons. Polarization diagram of (b) G peak, (c) D peak, (d) D′ peak, and (e) C–H peak. The red line and the black line represent the data after the revise and the original data, respectively.

**Table 1.** Raman shift identification of AGNRs.

| Raman shift ($cm^{-1}$) | Mode |
|---|---|
| 397 | RBLM |
| 955 | RBLM-3 |
| 1221 | C-H bend |
| 1258 | D′ |
| 1341 | D |
| 1601 | G |
| 2606 | D′+D |
| 2948 | D+G |

Large-scale STM images Fig. 4(a) show that CGNRs grow densely along the steps of the Au (11 11 12) surface. The CGNRs are distributed in parallel arrays on the same surface instead of epitaxy across the steps (Fig. 4(b)). The precursor (DBCh) is a chiral molecule on the substrate. Therefore, the CGNRs have heterogeneous structures due to the lack of selectivity in the growth process, which cannot grow into straight ribbons like AGNRs. Nevertheless, the growth of CGNRs on Au (11 11 12) still showed significant anisotropy, which

proved that the template effect of steps surface was still applicable to the non-linear GNRs. Figure 4(c) shows the polarized Raman spectrum of CGNRs. The existence of heterostructures in the GNRs makes the fine structure of the Raman spectrum invisible, while the high-intensity peaks diffused into wide peaks due to chemical shifts caused by different structures, which are similar to an amorphous structure.[31] As we can see, there is still some degree of polarization in the polarized Raman spectrum of CGNRs, but it is smaller compared to the AGNRs. Specifically, the $G_{\parallel}/G_{\perp}$ is only 2.1, much lower than of the $G_{\parallel}/G_{\perp}$ in the AGNRs.

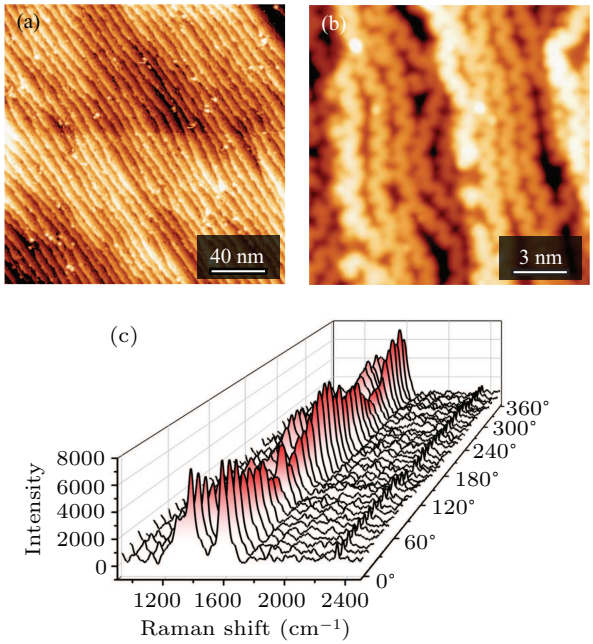



**Fig. 4.** Morphology and polarization Raman analysis of CGNRs. (a) The topographic STM image after the growth of the CGNRs, $I_t = 25$ pA, $U_s = 1$ V. (b) A zoom-in image clearly shows the presence of multiple heterostructures in the CGNRs, which makes the whole CGNRs twisted. (c) Polarized Raman spectrum of CGNRs.

In graphene nanoribbons, the TO and LO modes of the G peak degenerating result in cleavage of G peak. Kenichi Sasaki calculated that only the LO mode in AGNRs had Raman activity, while the TO mode in ZGNRs had Raman activity.[32] The CGNRs have two kinds of edges, which are armchair edges and zigzag edges, as shown in Fig. 5(b), which should have different G peak Raman active modes. We did observe significant G peak splitting in the Raman spectrum. By fitting the G peak with using a Lorentzian distribution, the G peak mainly split into the G+ peak around 1600 $cm^{-1}$ and a series of G– peaks around 1565 $cm^{1}$. The G peak at 10°, as an example, is contributed by two peaks around 1565 $cm^{-1}$ which we recognized as G– peaks and one peak at 1600 $cm^{-1}$ as G+ peak as shown in Fig. 5(a). Due to measurement noise and the effects of the complex edges of CGNRs, there is a small shift in the peak position of the G– peak in the Raman spectra at different angles. Considering that their wavenumbers are concentrated in a tiny range of 1550 $cm^{-1}$ (G– peak 1) ∼ 1575 $cm^{-1}$ (G– peak 2), we treat this collection of peaks as a G– peak group for further analysis. It is worth mentioning that due to the loud noise, we used the peak area to compare the intensity of each peak when analyzing the CGNRs Raman spectrum.

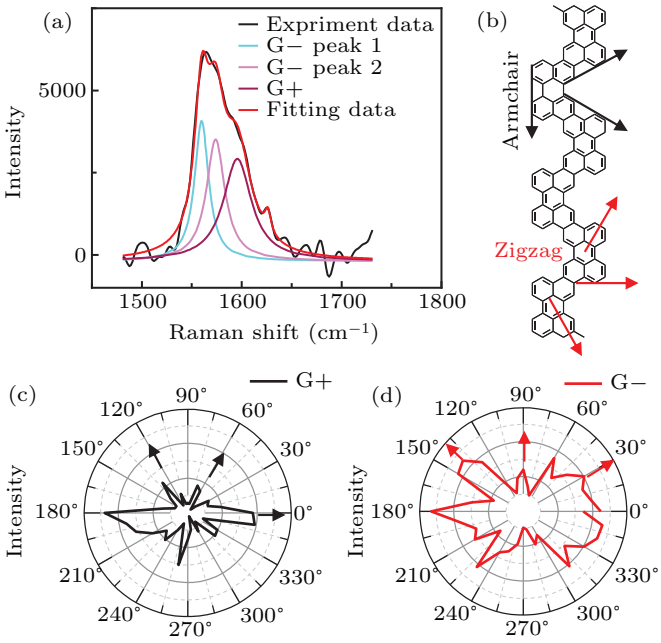



**Fig. 5.** G peak analysis of CGNRs. (a) G peak fitting of Raman spectrum at 10°. (b) Description of two kinds of edges in CGNRs. The black and red arrows mark the armchair boundary and the zigzag boundary of the CGNRs, respectively. (c) Normalized polarization diagram of Raman G+ peak. (d) The normalized polarization diagram of the Raman G peak.

Fitting G peaks of CGNRs polarized Raman spectra with a Lorentzian distribution at all angles, we obtained polarization diagrams of G+ and G– Raman peak areas. The G+ peak is around 1600 $cm^{-1}$ and the highest peak intensity appears around 0° and 180° as shown in Fig. 5(c). Considering that this is similar to AGNRs, we believe that the G+ peak is the LO mode of the CGNRs armchair edge. The other two armchair edges are shorter, which produces the weaker Raman peaks at around 60° and 120°, as shown in Fig. 5(d). G+ peak has a distinct polarization phenomenon, even stronger anisotropy than the anisotropy of the AGNRs LO mode.

On the other hand, the G– peak is stacked by a series of similar Raman peaks, making their polarization patterns very complicated. One of the biggest influences is the possibility of other nanoribbons due to the rotational freedom during the synthesis. If we consider the perfect CGNRs, it should have three zigzag edges. Therefore, the intensity of G– peak near 30°, 90° and 120°, as shown in Fig. 5(d) is contributed by zigzag edges. However, the existing intensity of G– peak at around 0° and 180° is yet to be explained.

The intensity of the G– peak at 0° and 180° is very similar to the G+ peak. Consider that the intensity of the G peak around 0° and 180° are contributed by the armchair edge. It is reasonable to infer that G– peak at 0° and 180° are also related

to the armchair edge. There are two possible explanations. The first is the G peak splitting caused by stress, which results in the red-shifted. Another possibility is that the LO mode of the armchair edge generates a red-shift due to Kohn anomalies (KAs).[32] However, the Raman spectra of AGNRs are entirely free of stress splitting, which indicates that the growth process of GNRs does not introduce stress. Then, the stress can only come from CGNRs themselves. That is, CGNRs as non-linear nanoribbons cannot form dense row structures on the substrate and the high coverage will cause the nanoribbons to squeeze each other, resulting in stress. Unfortunately, we are currently unable to measure and regulate this possible stress. If the LO mode of the armchair edge is red-shifted due to KAs, a similar problem is that the Raman spectrum of AGNRs does not observe the KAs red-shift. At the same time, it is challenging to regulate the Fermi level effectively to determine whether there are KAs. Therefore, the mechanism of the extra vibration mode is still an open question. We will consider these issues further in the future.

## 3. Conclusions

We successfully synthesized AGNRs and CGNRs arrays on Au (11 11 12) and measured their polarization Raman spectrum. The polarization Raman spectrum of AGNRs shows evident polarization. This nanoribbon array can be used at light modulators because of the polarization uniformity. The specific Raman vibration mode has no apparent influence on the polarization. The enhanced Raman spectra obtained by using this polarization effect can observe multiple double resonance Raman peaks of AGNRs, providing an excellent platform for theoretical research of double resonance Raman spectroscopy of GNRs. The polarization Raman spectrum of CGNRs is relatively weak. Therefore, using polarized Raman spectroscopy to detect the alignment of GNRs arrays is non-universal. The existence of multiple edges with different vibrational activity modes in CGNRs leads to complex variations in the intensity of Raman peaks at various angles. This indicates that the polarized Raman spectra of GNRs arrays have great potential to analyze the Raman active mode of complex GNRs.

## Appendix A: Methods

### A1. Synthesis

All synthesis steps are performed by the molecular beam epitaxy under an ultra-high vacuum with $1 \times 10^{-10}$ mbar. The clean Au (11 11 12) single crystal surface is etched by $Ar^+$ ions, then heated to 800 K and kept for 40 min to obtain high-quality clean terraces. The molecular precursors DBBA (10,10′-dibromo-9,9′-bianthracene, Sigma-Aldrich, >99% purity) and DBCh (6,12-dibromochrysene, Aladdin, > 97% purity) were deposited onto clean Au (11 11 12) single crystal surfaces held at 473 K. The crucibles filled with DBBA molecules and DBCh molecules were heated to evaporation temperatures of 373 K and 360 K, respectively. After deposition, the sample was annealed to 60 K for 30 min inducing the cyclo-dehydrogenation reaction to fabricate high-quality GNRs arrays.

### A2. STM measurement

Topographic scanning tunneling microscopy images of GNRs on Au (11 11 12) samples were characterized by a Scienta Omicron LT-STM operated around 4.2 K. Constant-current STM images were recorded with 1.0 V sample bias and 0.025 nA setpoint current.

### A3. Raman spectroscopy

Raman spectroscopy with a linearly polarized light wavelength of 532 nm was performed with a Renishaw inVia Qontor Confocal Raman microscope, operated at 5 mW light power. Three sweeps acquired spectra of AGNRs with 5 s of integration time and a 50× objective lens. Raman spectroscopy of CGNRs was obtained by three sweeps with 15 s of integration time and a 20× objective lens. Both GNRs have multi-angle polarization Raman using a homemade rotating sample holder.

## Acknowledgements

Project supported by the National Natural Science Foundation of China (Grant No. 61901200), the Yunnan Fundamental Research Projects (Grant Nos. 2019FD041, 202101AU070043, 202101AV070008, and 202101AW070010), the Strategic Priority Research Program of Chinese Academy of Sciences (Grant No. NXDB30010000), and the Dongguan Innovation Research Team Program.

## References

[1] Cai J, Ruffieux- P, Jaafar R, Bieri M, Braun T, Blankenburg S, Muoth M, Seitsonen A P, Saleh M, Feng X, Mullen K and Fasel R 2010 *Nature* **466** 470
[2] Cai J, Pignedoli C A, Talirz L, Ruffieux P, Sode H, Liang L, Meunier V, Berger R, Li R, Feng X, Mullen K and Fasel R 2014 *Nat. Nanotechnol.* **9** 896
[3] Groning O, Wang S, Yao X, Pignedoli C A, Borin Barin G, Daniels C, Cupo A, Meunier V, Feng X, Narita A, Mullen K, Ruffieux P and Fasel R 2018 *Nature* **560** 209
[4] Driver S M, Toomes R L and Woodruff D P 2016 *Surf. Sci.* **646** 114
[5] Sun S, Guan Y, Hao Z, Ruan Z, Zhang H, Lu J, Gao L, Zuo X and Cai J 2022 *Nano Res.* **15** 653
[6] Yang H, Cao Y, Gao Y, Fu Y, Huang L, Liu J, Feng X, Du S and Gao H-J 2021 *Chin. Phys. B* **30** 056802
[7] Wang X Y, Urgel J I, Barin G B, Eimre K, Di Giovannantonio M, Milani A, Tommasini M, Pignedoli C A, Ruffieux P, Feng X, Fasel R, Mullen K and Narita A 2018 *J. Am. Chem. Soc.* **140** 9104
[8] Su X, Xue Z, Li G and Yu P 2018 *Nano Lett.* **18** 5744
[9] Slota M, Keerthi A, Myers W K, Tretyakov E, Baumgarten M, Ardavan A, Sadeghi H, Lambert C J, Narita A, Mullen K and Bogani L 2018 *Nature* **557** 691

[10] Denk R, Hohage M, Zeppenfeld P, Cai J, Pignedoli C A, Sode H, Fasel R, Feng X, Mullen K, Wang S, Prezzi D, Ferretti A, Ruini A, Molinari E and Ruffieux P 2014 *Nat. Commun.* **5** 4253

[11] Sun K, Ji P, Zhang J, Wang J, Li X, Xu X, Zhang H and Chi L 2019 *Small* **15** 1804526

[12] Qin J, Xia S, Jia K, Wang C T, Tang T T, Lu H P, Zhang L, Zhou P H, Peng B, Deng L J and Bi L 2018 *Apl Photonics* **3** 016103

[13] Ohtomo M, Sekine Y, Hibino H and Yamamoto H 2018 *Appl. Phys. Lett.* **112** 021602

[14] Overbeck J, Barin G B, Daniels C, Perrin M L, Liang L B, Braun O, Darawish R, Burkhardt B, Dumslaff T, Wang X Y, Narita A, Mullen K, Meunier V, Fasel R, Calame M and Ruffieux P 2019 *Phys. Status Solidi B* **256** 1900343

[15] Linden S, Zhong D, Timmer A, Aghdassi N, Franke J H, Zhang H, Feng X, Mullen K, Fuchs H, Chi L and Zacharias H 2012 *Phys. Rev. Lett.* **108** 216801

[16] Passi V, Gahoi A, Senkovskiy B V, Haberer D, Fischer F R, Gruneis A and Lemme M C 2018 *ACS Appl. Mater. Interfaces* **10** 9900

[17] Cong C, Yu T and Wang H 2010 *ACS Nano* **4** 3175

[18] Ferreira E H M, Moutinho M V O, Stavale F, Lucchese M M, Capaz R B, Achete C A and Jorio A 2010 *Phys. Rev. B* **82** 125429

[19] Verzhbitskiy I A, Corato M D, Ruini A, Molinari E, Narita A, Hu Y, Schwab M G, Bruna M, Yoon D, Milana S, Feng X, Mullen K, Ferrari A C, Casiraghi C and Prezzi D 2016 *Nano Lett.* **16** 3442

[20] Annese E, Viol C E, Zhou B, Fujii J, Vobornik I, Baldacchini C, Betti M G and Rossi G 2007 *Surf. Sci.* **601** 4242

[21] Luo G F, Wang L, Li H, Qin R, Zhou J, Li L Z, Gao Z X, Mei W N, Lu J and Nagase S 2011 *J. Phys. Chem. C* **115** 24463

[22] Fritton M, Duncan D A, Deimel P S, Rastgoo-Lahrood A, Allegretti F, Barth J V, Heckl W M, Bjork J and Lackinger M 2019 *J. Am. Chem. Soc.* **141** 4824

[23] Senkovskiy B V, Pfeiffer M, Alavi S K, Bliesener A, Zhu J, Michel S, Fedorov A V, German R, Hertel D, Haberer D, Petaccia L, Fischer F R, Meerholz K, van Loosdrecht P H M, Lindfors K and Gruneis A 2017 *Nano Lett.* **17** 4029

[24] Malard L M, Pimenta M A, Dresselhaus G and Dresselhaus M S 2009 *Phys. Rep.* **473** 51

[25] Sasaki K, Yamamoto M, Murakami S, Saito R, Dresselhaus M S, Takai K, Mori T, Enoki T and Wakabayashi K 2009 *Phys. Rev. B* **80** 155450

[26] Saito R, Furukawa M, Dresselhaus G and Dresselhaus M S 2010 *J. Phys. Condens Matter* **22** 334203

[27] Gillen R, Mohr M and Maultzsch J 2010 *Phys. Status Solidi B* **247** 2941

[28] Vandescuren M, Hermet P, Meunier V, Henrard L and Lambin P 2008 *Phys. Rev. B* **78** 195401

[29] Hasdeo E H, Nugraha A R T, Dresselhaus M S and Saito R 2016 *Phys. Rev. B* **94** 075104

[30] Frank O, Mohr M, Maultzsch J, Thomsen C, Riaz I, Jalil R, Novoselov K S, Tsoukleri G, Parthenios J, Papagelis K, Kavan L and Galiotis C 2011 *ACS Nano* **5** 2231

[31] Ferrari A C and Rbertson J 2000 *Phys. Rev. B* **61** 14095

[32] Mohiuddin T, Lombardo A, Nair R, Bonetti A, Savini G, Jalil R, Bonini N, Basko D, Galiotis C and Marzari N 2009 *Phys. Rev. B* **79** 205433